

RobustPeriod: Time-Frequency Mining for Robust Multiple Periodicities Detection

Qingsong Wen, Kai He, Liang Sun, Yingying Zhang, Min Ke, Huan Xu
Machine Intelligence Technology, DAMO Academy, Alibaba Group
Bellevue, Washington, USA
{qingsong.wen,kai.he,liang.sun,congrong.zyy,dawu,huan.xu}@alibaba-inc.com

ABSTRACT

Periodicity detection is an important task in time series analysis as it plays a crucial role in many time series tasks such as classification, clustering, compression, anomaly detection, and forecasting. It is challenging due to the following reasons: 1) complicated non-stationary time series; 2) dynamic and complicated periodic patterns, including multiple interlaced periodic components; 3) outliers and noises. In this paper, we propose a robust periodicity detection algorithm to address these challenges. Our algorithm applies maximal overlap discrete wavelet transform to transform the time series into multiple temporal-frequency scales such that different periodicities can be isolated. We rank them by wavelet variance and then at each scale, and then propose Huber-periodogram by formulating the periodogram as the solution to M-estimator for introducing robustness. We rigorously prove the theoretical properties of Huber-periodogram and justify the use of Fisher's test on Huber-periodogram for periodicity detection. To further refine the detected periods, we compute unbiased autocorrelation function based on Wiener-Khinchin theorem from Huber-periodogram for improved robustness and efficiency. Experiments on synthetic and real-world datasets show that our algorithm outperforms other popular ones for both single and multiple periodicity detection. It is now implemented and provided as a public online service at Alibaba Group and has been used extensive in different business lines.

CCS CONCEPTS

• **Mathematics of computing** → Time series analysis; • **Information system** → Data mining.

KEYWORDS

time series, periodicity detection, multiple periods, time-frequency mining

1 INTRODUCTION

The explosive growth of IoT and many other applications lead to huge amounts of the time series data. Many time series are characterized by repeating cycles, or periodicity. For example, many human activities show periodic behavior, such as the human cardiac cycle and the traffic congestion in daily peak hours. As periodicity is an important feature of time series, periodicity detection or mining, is crucial in many time series tasks, such as forecasting [25], anomaly detection [21], classification [28], clustering [27], and compression [22]. Accurate periodicity detection not only enables better processing of the single time series, it also facilitates the study of multiple time series. For example, we can define similarity based

on periodicity patterns between multiple time series, which can be used in further analysis such as classification and clustering.

Accurate periodicity detection is challenging due to the diversity and complexity of different real-world time series data. Firstly, most real-world time series is non-stationary and other components such as trend can make periodicity detection difficult. Secondly, the periodic patterns could be complicated and dynamic. On the one hand, the periodic pattern can change or deviate the typical pattern over time. For example, the daily periodic pattern of the daily sales of a main online shopping retailer on black Friday can deviate significantly from its typical daily behavior. On the other hand, multiple interlaced periodicities can appear together, which makes this problem more complicated. For example, the traffic congestion time series typically exhibits daily and weekly periodicities, but the weekly pattern may change when long weekend happens. Thirdly, time series data generally contains different types of noises and outliers, which makes the robust detection challenging. In particular, many existing methods fail when outliers last for some time.

Periodicity detection has a long history in a variety of different fields, including data mining [28], statistics [1], astronomy [8], bioinformatics [32], etc. Among various methods proposed for periodicity detection, two most popular types of methods are: 1) frequency domain methods identifying the underlying periodic patterns by transforming time series into the frequency domain; 2) time domain methods correlating the signal with itself via autocorrelation function (ACF). Specifically, the discrete Fourier transform (DFT) converts a time series from the time domain to the frequency domain, resulting in the so-called periodogram which encodes the strength at different frequencies. Usually the top- k dominant frequencies are investigated to find the frequencies corresponding to periodicities. A problem of periodogram is the so-called spectral leakage [28], which causes frequencies not integer multiples of DFT bin width to disperse over the spectrum. Also the periodogram is not robust to abrupt trend changes and outliers, and not accurate for short periods. On the other hand, autocorrelation tends to reveal insights for large periods but is prone to outliers and noises. Also, both DFT and ACF fail to process time series with multiple periodicities robustly and effectively. The periodogram may give misleading information when multiple interlaced periodicities exist. Recently some algorithms combining DFT and ACF have been proposed [28]. Unfortunately, they cannot address all the aforementioned challenges.

In this paper we propose a new periodicity detection method called RobustPeriod to detect multiple periodicities robustly and accurately. To mitigate the side effects introduced by trend, spikes

and dips, we introduce the Hodrick-Prescott (HP) trend filtering [9] to detrend and smooth the data. We apply the maximal overlap discrete wavelet transform (MODWT) to decouple time series into multiple levels of wavelet coefficients and then detect single periodicity at each level. We propose a method to robustly calculate unbiased wavelet variance at each level to rank periodic possibilities to speed up the computation. For those with highest possibility of periodic patterns, we propose a robust Huber-periodogram and apply Fisher's test to select the candidates of periodic lengths. We rigorously prove the theoretical properties of Huber-periodogram and justify the use of Fisher's test based on Huber-periodogram. Compared with the periodogram generated in traditional spectral methods, our Huber-periodogram can effectively deal with impulse random errors with unknown heavy-tailed error distributions. Finally, we apply the robust ACF to validate these period length candidates. By applying Wiener-Khinchin theorem, the unbiased robust ACF can be computed efficiently and accurately based on the Huber-periodogram, and then more accurate period length(s) can be detected. Compared with various state-of-the-art periodicity detection algorithms, our RobustPeriod algorithm performs significantly better on both synthetic and real-world datasets. Due to its good performance especially in real-world scenarios, it is now implemented and provided as a public online service at Alibaba Group.

2 RELATED WORK

The common periodicity detection can be categorized into two groups: 1) frequency domain methods relying on periodogram after Fourier transform; 2) time domain methods relying on autocorrelation function (ACF). Note that periodicity detection is also referred as seasonality detection or season length estimation [26], we use periodicity and seasonality in this paper equivalently.

In the frequency domain methods, the periodogram measures how periodic the time series is at different frequencies. If a time series does not contain a periodic component, then the peak values of periodogram are not significant. However, periodogram is not accurate when the period length is long or the time series is with sharp edges. In the time domain methods, the ACF measures the similarity between a sequence and itself for some lags. Intuitively, a time series is periodic with a period T if it can be divided into equal segments with length T sharing high similarities. In other words, the ACF whose lag is the multipliers of T would be locally maximum or peaks. Based on this properties of ACF, numerous methods have been proposed, including the analysis of autocorrelation peaks [30], autocorrelation zero-distance [26]. However, the estimation of ACF and the automated discovery of its maximum values can be affected by outliers and noises easily, which leads to many false alarms in practice.

Some methods have been proposed in the joint frequency-time domain to combine the advantages of both methods. In AUTOPEIOD [18, 28], it first selects a list of candidates in the frequency domain using periodogram, and then identifies the exact period in the time domain using ACF. The intuitive idea is that a valid period from the periodogram should lie on a hill of ACF. [26] proposes an ensemble method called SAZED which combines multiple periodicity detection methods together. Compared with AUTOPERIOD, it

selects the list of candidate periods using both frequency domain methods and time domain methods. Also different properties of autocorrelation of periodic time series are utilized to validate period. Unfortunately, it can only detect single period. In terms of multiple periodicity detection, a related topic is the pitch periodicity detection [29] where multiple periodicities are associated with the fundamental frequency (F0). In fact, the periodic waveform repeats at F0 and can be decomposed into multiple components which have frequencies at integer multiples of the F0. In our scenarios, we may not have the fundamental frequency and the relationship between different frequencies can be more complicated.

Recently some other periodicity detection algorithms have been proposed in the field of data mining, signal processing and astrology. One improvement [19] is proposed to handle non-stationary time series using a sliding window and track the candidate periods using a Kalman filter, but it is not universally applicable and not robust to outliers. In [16], a method immune to noisy and incomplete observations is proposed, but it can only handle binary sequences. [35] also proposes a method to detect multiple periodicities. Unfortunately, it only works on discrete event sequences. Some other types of periodicity detection algorithms in the literature include wavelet transform based method [1], dynamic time warping based method [6], epoch folding [8], etc.

In terms of the statistical tests used for periodicity detection, two traditional tests are Fisher's test [7] for a single periodicity and Siegel's test [15, 24] for multiple periodicities. Fisher's test adopts the Fourier periodogram to calculate the g -statistic by using the maximum periodogram coordinate. The Siegel's test generalizes the Fisher's test by considering all large periodogram values to overcome the multiple peak problem when multiple periodicities occur. However, these methods are not robust to outliers and often generate false positive in complex time series.

3 METHODOLOGY

3.1 Framework Overview

We consider the following time series model with trend and multiple seasonalities/periodicities as

$$y_t = \tau_t + \sum_{i=1}^m s_{i,t} + r_t, \quad t = 0, 1, \dots, N-1 \quad (1)$$

where y_t represents the observed time series at time t , τ_t denotes the trend component, $s_t = \sum_{i=1}^m s_{i,t}$ is the summation of multiple seasonal/periodic components with periods as $T_i, i = 1, \dots, m$, $r_t = a_t + n_t$ denotes the remainder part which contains the noise n_t and possible outlier a_t , and m is the number of periodic components. For periodicity detection in this paper, we aim to identify the number of the periodic components and each period length.

Intuitively, our periodicity detection algorithm first isolates different periodic components, and then verifies single periodicity by robust Huber-periodogram and Huber-ACF. Specifically, RobustPeriod consists of three main components as shown in Fig. 1: 1) data preprocessing; 2) decoupling (potential) multiple periodicities by MODWT; 3) robust single periodicity detection by Huber-periodogram and Huber-ACF.

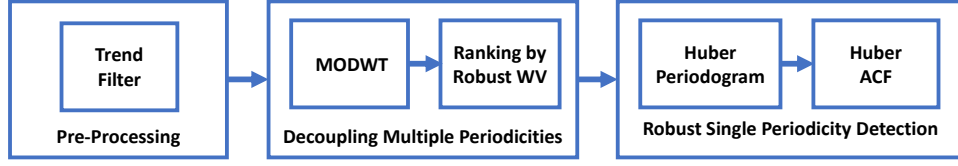


Figure 1: Framework of the proposed RobustTrend algorithm.

3.2 Data Preprocessing

The complex time series in real-world may have varying scales and trends under the influence of noise and outliers. In the first step, we perform data preprocessing like data normalization and detrending. Here we highlight time series detrending as the trend component would bias the estimation of ACF, resulting in misleading periodic information. Specifically, we adopt the Hodrick-Prescott (HP) trend filtering [9] to estimate the trend $\hat{\tau}_t$ due to its good performance and low computational cost:

$$\hat{\tau}_t = \arg \min_{\tau_t} \frac{1}{2} \sum_{t=0}^{N-1} (y_t - \tau_t)^2 + \lambda \sum_{t=1}^{N-2} (\tau_{t-1} - 2\tau_t + \tau_{t+1})^2. \quad (2)$$

After estimating the trend $\hat{\tau}_t$, the detrended time series is

$$y'_t = y_t - \hat{\tau}_t. \quad (3)$$

3.3 Robust MODWT: Decouple Multiple Periodicities

3.3.1 Daubechies MODWT for time series decomposition. We adopt maximal overlap discrete wavelet transform (MODWT) to decompose the input time series into multiple time series at different levels to facilitate periodicity detection. The motivation to use MODWT instead of DWT is due to the advantages of MODWT: 1) ability to handle any sample size; 2) increased resolution at coarser scales; 3) a more asymptotically efficient wavelet variance estimator than DWT; 4) can handle non-stationary time series and non-Gaussian noises more effectively.

Here we adopt the common Daubechies wavelet based MODWT [5, 20] for time series analysis. When the MODWT is performed on time series y'_t , the j th level wavelet and scaling coefficients $w_{j,t}$ and $v_{j,t}$ are given by

$$w_{j,t} = \sum_{l=0}^{L_j-1} h_{j,l} y'_{t-l \bmod N}, \quad v_{j,t} = \sum_{l=0}^{L_j-1} g_{j,l} y'_{t-l \bmod N}, \quad (4)$$

where $\{h_{j,l}\}_{l=0}^{L_j-1}$, $\{g_{j,l}\}_{l=0}^{L_j-1}$ are j th level wavelet filter and scaling filter, respectively, and the filter width is $L_j = (2^j - 1)(L_1 - 1) + 1$ with L_1 as the width of unit-level Daubechies wavelet coefficients [5]. Note that the wavelet filter $h_{j,l}$ in Eq. (4) performs band-pass filter with nominal passband as $1/2^{j+1} \leq |f| \leq 1/2^j$. Therefore, if there is a periodic component of the time series y'_t located in the nominal passband $1/2^{j+1} \leq |f| \leq 1/2^j$, this periodic component would be filtered into the j th level wavelet coefficient. Therefore, we can decouple multiple periodicities by adopting MODWT where the possible period length of j th level wavelet coefficients is within length of $[2^j, 2^{j+1}]$, as illustrated in Fig. 2.

In real-world scenarios due to outliers and noise, time series is usually non-stationary and the noise is not Gaussian. But the MODWT can overcome these shortcomings to some extent. Suppose that y'_t is d th order stationary time series, which means y'_t is a non-stationary but its d th order backward difference $y_t^{(d)} = \sum_{k=0}^d \frac{(-1)^k d!}{k!(d-k)!} y'_{t-k}$ is stationary. Note that a special case of d th order stationary process is ARIMA(p, d, q) which is a widely used model in time series analysis. Let define a particular wavelet coefficient process $\tilde{w}_{j,t} = \sum_{l=0}^{L_j-1} h_{j,l} y'_t$. we can see that $\tilde{w}_{j,t}$ equals the wavelet coefficient $w_{j,t}$ in Eq. (4) for $t \geq L_j - 1$ (i.e., non-boundary coefficients). Then, we have the following property for MODWT:

PROPOSITION 3.1. *If the wavelet filter length $L_1 \geq 2d$, then $\tilde{w}_{j,t}$ is a stationary process and only has short-term dependence with power spectral density (PSD) given by*

$$S_j(f) = \frac{\left| \sum_{l=0}^{L_j-1} h_{j,l} e^{-j2\pi f l} \right|^2 S_{y_t^{(d)}}(f)}{(4 \sin^2(\pi f))^d},$$

where $S_{y_t^{(d)}}(f)$ is PSD of $y_t^{(d)}$ [36].

Furthermore, if y'_t is a non-Gaussian process, the wavelet coefficients of Daubechies MODWT can also be near Gaussian thanks to the following proposition:

PROPOSITION 3.2. *For certain non-Gaussian processes, the wavelet coefficient $w_{j,t}$ is approximately Gaussian (particularly for large level j) because linear filtering tends to induce Gaussianity [17].*

Therefore, even the time series is a non-Gaussian process with long memory and high degree of correlation, the wavelet coefficients from MODWT can be approximately Gaussian, uncorrelated and stationary, which would improve the performance of periodicity detection for time series.

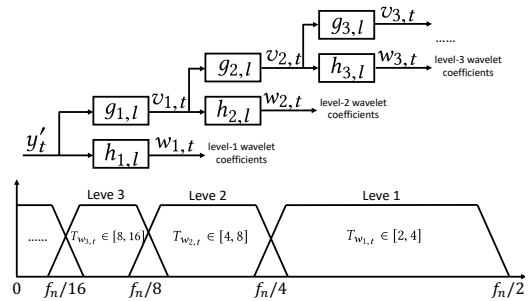


Figure 2: Principle of adopting MODWT for decoupling multiple periodicities.

3.3.2 Robust Unbiased Wavelet Variance. Besides decoupling multiple periods of time series, another benefit of MODWT is that the corresponding wavelet variance estimation helps to locate the periodic component of time series in the frequency bands as it is actually a rough estimate of the PSD. Thus, we can rank possible single periodic components by their corresponding wavelet variances.

For level J_0 decomposition, based on the energy preserving of MODWT, we have $\|y'\|^2 = \sum_{j=1}^{J_0} \|\mathbf{w}_j\|^2 + \|\mathbf{v}_{J_0}\|^2$, which leads to wavelet variance decomposition as $\hat{\sigma}_{y'}^2 = \sum_{j=1}^{J_0} \hat{\sigma}_{\mathbf{w}_j}^2 + \hat{\sigma}_{\mathbf{v}_{J_0}}^2$ where $\hat{\sigma}_{\mathbf{w}_j}^2$, $\hat{\sigma}_{\mathbf{v}_{J_0}}^2$ are the j th level empirical wavelet variance and level J_0 empirical scaling variance, respectively. If y'_t is stationary, then $\hat{\sigma}_{y'}^2 = \sum_{j=1}^{\infty} \hat{\sigma}_{\mathbf{w}_j}^2$. Therefore, wavelet variance provides a scale-based analysis of variance (ANOVA) for time series, which can offer an intuitive explanation of how a time series is structured.

We adopt biweight midvariance as the estimation of wavelet variance due to its robustness and efficiency [34]. Furthermore, the first $L_j - 1$ wavelet coefficients are excluded for the aim of unbiased variance estimation, since the wavelet transform introduces periodic extension as defined in Eq. (4). Therefore, we use the following formulation for robust unbiased estimation of wavelet variance:

$$\hat{v}_{\mathbf{w}_j}^2 = \frac{M_j \sum_{t=L_j-1}^{N-1} (\mathbf{w}_{j,t} - \text{Med}(\mathbf{w}_{j,t}))^2 (1 - u_t^2)^4 I(|u_t| < 1)}{\left(\sum_{t=L_j-1}^{N-1} (1 - u_t^2)(1 - 5u_t^2) I(|u_t| < 1) \right)^2},$$

where $I(x)$ is the indicator function, u_t is calculated as $u_t = (\mathbf{w}_{j,t} - \text{Med}(\mathbf{w}_{j,t})) / (9 \cdot \text{MAD}(\mathbf{w}_{j,t}))$, $M_j = N - L_j + 1$ is the number of nonboundary coefficients at the j th level, and $\text{Med}(\mathbf{w}_{j,t})$ and $\text{MAD}(\mathbf{w}_{j,t})$ are median and mean absolute deviation (MAD) of $\mathbf{w}_{j,t}$, respectively.

For the j th level wavelet variance estimation, its wavelet variance is approximately equal to the integral of the PSD at the nominal octave passband as $1/2^{j+1} \leq |f| \leq 1/2^j$, i.e.,

$$\hat{v}_{\mathbf{w}_j}^2 \approx \int_{1/2^{j+1} \leq |f| \leq 1/2^j} S_{y'}(f) df.$$

It can be concluded that if there is a periodic component filtered into the j th level wavelet coefficient, a large value of $\hat{\sigma}_{\mathbf{w}_j}^2$ would be expected. Therefore, we can rank the wavelet coefficients based on their wavelet variances. Then, the order of single-period detection in each wavelet coefficient can follow this ranking to output the most significant period first.

3.4 Robust Single Periodicity Detection

3.4.1 Robust Huber-Periodogram based Fisher's Test for Generating Periodicity Candidates. In this subsection we design a robust Huber-periodogram based Fisher's test for improved single periodicity detection. We also provide the theoretical properties of the Huber-periodogram.

First, we double the length of wavelet coefficient \mathbf{w}_j of each level by padding N zeros denoted as $\mathbf{x}_j = [\mathbf{w}_j^T, 0, \dots, 0]^T$, where the length of \mathbf{x}_j is $N' = 2N$. The purpose of this padding operation is to obtain robust ACF through Huber-periodogram (will be shown later). In the following, we drop the level index j for simplification.

To detect the hidden periodicity, Fisher's test [7] defines the g -statistic as

$$g = \frac{\max_k P_k}{\sum_{j=1}^N P_j}, \quad j = 1, 2, \dots, N, \quad (5)$$

where P_k is the periodogram based on DFT and it is defined as

$$P_k = \|\text{DFT}\{x_t\}\|^2 = \frac{1}{N'} \sum_{t=0}^{N'-1} \left\| x_t e^{-i2\pi kt/N'} \right\|^2, \quad (6)$$

where $i = \sqrt{-1}$. The Fisher's test in Eq. (5) sets a null hypothesis H_0 that the time series is generated by a Gaussian white noise sequence, against the alternative hypothesis H_1 that the data is generated by a Gaussian white noise sequence with a superimposed deterministic periodic component. Under the hypothesis H_0 of Gaussian white noise with variance σ^2 , the distribution of periodogram can be obtained as a chi-square distribution with 2 degrees of freedom, i.e., $P_k \sim (1/2)\sigma^2 \chi^2(2)$. Therefore, the distribution of g -statistic under hypothesis H_0 can be expressed as [7]

$$P(g \geq g_0) = 1 - \sum_{k=1}^{\lfloor 1/g_0 \rfloor} \frac{(-1)^{k-1} N!}{k!(N-k)!} (1 - kg_0)^{N-1},$$

which gives a p -value to determine if a time series is periodic. If this value is less than the predefined threshold α , we reject the null hypothesis H_0 and conclude the time series have a period component with periodicity as N/k where $k = \arg \max_k P_k$.

To make the estimated periodogram more robust, we introduce the so-called Huber-periodogram. The key idea is to formulate the periodogram as an equivalent least squares problem, and replace the least squares by M-estimator. Specifically, the periodogram of Eq. (6) can be equivalently computed by solving

$$P_k = \frac{N'}{4} \left| \hat{\beta}_{LS}(k) \right|^2 = \frac{N'}{4} \left| \arg \min_{\beta \in \mathbb{R}^2} \|\phi \beta - \mathbf{x}\|^2 \right|^2, \quad (7)$$

where $\hat{\beta}_{LS}(k)$ is the least square estimation of harmonic regressor $\phi_t = [\cos(2\pi kt/N'), \sin(2\pi kt/N')]^T$, ϕ and \mathbf{x} are the matrix forms of $[\phi_0, \phi_1, \dots, \phi_{N'-1}]^T$ and $\mathbf{x} = [x_0, x_1, \dots, x_{N'-1}]^T$, respectively. Based on Eq. (7), we could replace the sum-of-squares loss function with the family of functions used in M-estimator, leading to the so-called robust M-periodogram [13]:

$$P_k^M = \frac{N'}{4} \left| \hat{\beta}_M(k) \right|^2 = \frac{N'}{4} \left| \arg \min_{\beta \in \mathbb{R}^2} \gamma(\phi \beta - \mathbf{x}) \right|^2, \quad (8)$$

where $\gamma(\mathbf{x})$ is a robustifying objective function defined as $\gamma(\mathbf{x}) = \sum_{t=0}^{N'-1} \gamma(x_t)$. When using least absolute deviation (LAD) loss for the robustifying function, we can get LAD-periodogram [13]. Instead, here we propose to adopt Huber loss [10] in Eq. (8) to get Huber-periodogram. The Huber loss is a combination of the sum-of-squares loss and the LAD loss, which is quadratic on small errors but grows linearly for large values of errors. Thus, it is robust and adaptive on different types of data. In addition, the Huber-periodogram can lead to robust ACF, which is beneficial for validating final periodicity. Specifically, the $\gamma(x)$ for Huber-periodogram is defined as

$$\gamma(x) = \gamma_{\zeta}^{hub}(x) = \begin{cases} \frac{1}{2}x^2, & |x| \leq \zeta \\ \zeta|x| - \frac{1}{2}\zeta^2, & |x| > \zeta \end{cases} \quad (9)$$

The Huber-periodogram in Eq. (8) can be efficiently solved by ADMM [4] method, and the the distribution of the P_k^M has the following proposition:

PROPOSITION 3.3. *Under some practical mild conditions for the time series \mathbf{x} , as $n \rightarrow \infty$, we have*

$$P_k^M \stackrel{A}{\sim} (1/2)m_2 S_2 \chi_2^2, \quad (10)$$

where the sign $\stackrel{A}{\sim}$ represents “asymptotically distributed as”, and the m_2 is the second moment of $\{x_t\}$, and $S_2 := \sum_{\tau=-\infty}^{\infty} r_2(\tau) \cos(\frac{2\pi k\tau}{n}) > 0$ with absolutely summable autocorrelation function $r_2(\tau)$ for process $\{g_2(x_t)\}$, with $g_2(x) := |x| \text{sgn}(x)$.

PROOF. Let $\hat{\beta}_M(\mathbf{k})$ be the minimizer of the problem:

$$\hat{\beta}_M(\mathbf{k}) := \arg \min_{\beta \in \mathbb{R}^2} \sum_{t=1}^{N'} \gamma(\phi_t \beta - x_t), \quad (11)$$

where $\gamma(\cdot)$ is defined in (9). Assume that $\{x_t\}$ satisfies the following conditions:

- a) The $\{x_t\}$ have a common univariate probability density function $f(x)$ which is bounded and satisfies $m_2 := E(|x_t|^2) = \int |x|^2 f(x) dx < \infty$.
- b) The $\{x_t\}$ are ϕ -mixing with mixing coefficients $\phi(\tau)$ satisfying $\sum_{\tau=1}^{\infty} \sqrt{\phi(\tau)} < \infty$.
- c) The process $\{g_2(x_t)\}$, with $g_2(x) := |x| \text{sgn}(x)$, is stationary in second moments with zero mean and absolutely summable autocorrelation function $r_2(\tau)$ such that $S_2 := \sum_{\tau=-\infty}^{\infty} r_2(\tau) \cos(\frac{2\pi k\tau}{n}) > 0$.
- d) Let n_1 be the length of subsequence $\{x_{t_1}\} \subset \{x_t\}$, $|x_{t_1} - \phi_{t_1} \beta| \leq \zeta$ and n_2 be the length of subsequence $\{x_{t_2}\} \subset \{x_t\}$, $|x_{t_2} - \phi_{t_2} \beta| > \zeta$, we have $n_1 \geq n_2^2$.

Then as $N' \rightarrow \infty$, $\sqrt{N'} \hat{\beta}_M(\mathbf{k}) \stackrel{A}{\sim} N(0, 2m_2 S)$, and $P_k^M \stackrel{A}{\sim} (1/2)m_2 S_2 \chi_2^2$, where $P_k^M := \frac{N'}{4} \|\hat{\beta}_M(\mathbf{k})\|^2$, $S = \text{diag}\{S_2, S_2\}$ and sign $\stackrel{A}{\sim}$ represents “asymptotically distributed as”.

First, we show that with assumptions (a), (b) and (d), we have as $N' \rightarrow \infty$, $\sqrt{N'}(\hat{\beta}_M(\mathbf{k}) - \beta_0 - \theta_{N'}) \stackrel{A}{\sim} N(0, \Gamma_{N'})$, where $\theta_{N'} := \mathbf{Q}_{N'}^{-1} \mathbf{b}_{N'}$ and $\Gamma_{N'} := \mathbf{Q}_{N'}^{-1} \mathbf{W}_{N'} \mathbf{Q}_{N'}^{-1}$. Definitions of β_0 , $\mathbf{Q}_{N'}$, $\mathbf{W}_{N'}$ and $\mathbf{b}_{N'}$ are omitted here, which can be found in Appendix I of [14] where the asymptotic distribution of L_p -norm periodogram is studied for $p \in (1, 2)$. In the following, we drop the notation dependence of j for simplicity.

To get the optimal regression coefficient $\hat{\beta}_M(k)$, we need to solve optimization problem (11). Define two sequences $t^1 := \{t | |x_t - \phi_t \beta| \leq \zeta\}$, and $t^2 := \{t | |x_t - \phi_t \beta| > \zeta\}$. Let the total error to model x_t be $U_t := x_t - \phi_t \beta_0$. Because $x_t = U_t + \phi_t \beta_0$, it follow that $\hat{\beta}_M(k)$ also minimizes $\frac{1}{2} \sum_{t \in t^1} (|U_t - v_t(\delta)|^2 - |U_t|^2) + \frac{1}{2} \sum_{t \in t^2} (|U_t - v_t(\delta)| - |U_t|)$, with $\delta := \sqrt{N'}(\beta - \beta_0)$ and $v_t(\delta) := \phi_t \delta / \sqrt{N'}$. This problem can be reformulated as

$$Z_{N'}(\delta) = \frac{1}{2} \sum_{t \in t^1} (|U_t - v_t(\delta)|^2 - |U_t|^2) + \frac{1}{2} \sum_{t \in t^2} (|U_t - v_t(\delta)| - |U_t|). \quad (12)$$

We now want to show that $Z_{N'}(\delta)$ can be approximated by a quadratic function as

$$Z_{N'}(\delta) = \tilde{Z}_{N'}(\delta) + o_P(1) \quad (13)$$

for fixed δ . Based on Lemma 2.8 in [2], since the result (vii) in Lemma 2.8 holds for both $p = 1$ and 2, we are able to show that

$$\tilde{Z}_{N'}(\delta) = \sum_{t \in t^1} \{-g_2(U_t) v_t + \frac{1}{2} h_2(U_t) v_t^2 + r_2(U_t, v_t)\} + \frac{1}{2} \sum_{t \in t^2} \{-g_1(U_t) v_t + \frac{1}{2} h_1(U_t) v_t^2 + r_1(U_t, v_t)\}, \quad (14)$$

where $h_p(x) := (p-1)|x|^{p-2}$, and

$$r_i(u, v) := \min\{|u|^{i-3}|v|^3, |u|^{i-2}|v|^2\}, i = 1, 2. \quad (15)$$

Similar to [14], we can rewrite the above equation for $\tilde{Z}_{N'}(\delta)$ as

$$\tilde{Z}_{N'}(\delta) = T_{1N'} + T_{2N'} + T_{3N'}, \quad (16)$$

where $T_{1N'} := -\sum_{t \in t^1} g_2(U_t) v_t$, $T_{2N'} := \frac{1}{2} \sum_{t \in t^1} h_2(U_t) v_t^2$, and $T_{3N'} := \sum_{t \in t^1} r_2(U_t, v_t) + \frac{1}{2} \sum_{t \in t^2} (-g_1(U_t) v_t + r_1(U_t, v_t))$. The goal here is to assert that $Z_{N'}(\delta) - T_{1N'} - (1/2) \delta^T \mathbf{Q}_{N'} \delta = o_P(1)$, and $T_{1N'} = -\delta \zeta_{N'} \stackrel{A}{\sim} N(-\sqrt{N'} \delta^T \mathbf{b}_{N'}, \delta^T \mathbf{W}_{N'} \delta)$. Then the result as $N' \rightarrow \infty$, $\sqrt{N'} \hat{\beta}_M(\mathbf{k}) \stackrel{A}{\sim} N(0, 2m_2 S)$ follows directly. Since steps to show $T_{1N'}$ is asymptotically Gaussian and $T_{2N'}$ can be approximated by a quadratic function is similar to Appendix I of [14], we omit them here and focus on proving that $T_{3N'}$ is asymptotically negligible.

To prove $\sum_{t \in t^1} r_2(U_t, v_t) + \frac{1}{2} \sum_{t \in t^2} r_1(U_t, v_t)$ asymptotically goes to $o_P(1)$, we borrow the upper bounds that have been derived for $r_i(u, v)$, $i = 1, 2$ by [14], i.e., with $f_0 := \sup f(x)$

$$E\{r_1(U_t, v_t)\} \leq v_t^2 \cdot (f_0 \int_{|x| \leq |v_t| \& |x-v_t| \geq \zeta} |x|^{-1} dx + f_0 v_t \int_{|x| \geq |v_t| \& |x-v_t| \geq \zeta} x^{-2} dx). \quad (17)$$

$$E\{r_2(U_t, v_t)\} \leq v_t^2 \cdot (f_0 \int_{|x| \leq |v_t| \& |x-v_t| \leq \zeta} |x|^0 dx + f_0 v_t \int_{|x| \geq |v_t| \& |x-v_t| \leq \zeta} |x|^{-1} dx). \quad (18)$$

Given our piece-wise nature of Huber loss, it is easy to show that for both $p = 1$ and $p = 2$, the terms in parenthesis of (17) and (18) are finite with closed-form because the use of ζ with Huber loss function. Therefore, $E\{r_i(U_t, v_t)\}$ is bounded by $o_P(N'^{-1})$. Furthermore, under assumption (d) that $n_1 \geq n_2^2$, we have $\sum_{t \in t^2} -g_1(u) v$ in $T_{3N'}$ is $o_P(n_2 / \sqrt{n_1 + n_2}) \approx o_P(1)$. Therefore, we proof that $T_{3N'}$ is asymptotically negligible. Finally, Proposition 3.3 is a direct result under assumption (c) when $\beta_0 = \theta_{N'} = 0$. \square

Proposition 3.3 indicates that the Huber-periodogram behaves similarly to the vanilla periodogram as $n \rightarrow \infty$. Therefore, the Fisher's test based on Huber-periodogram can also be utilized to detection periodicity.

3.4.2 Robust Huber-Periodogram based ACF for Validating Periodicity Candidates. After obtaining period candidate from the robust Fisher’s test for each wavelet coefficient, we next validate each candidate and improve its accuracy by using ACF. This step is necessary since periodogram has limited resolution and spectral leakage may exist [28], which makes the candidate from Fisher’s test not accurate.

For the ACF of the time series from wavelet coefficient $w_{j,t}$ (denote as w_t for simple notation), the normalized estimation [3] is

$$ACF(t) = \frac{1}{(N-t)\delta_w^2} \sum_{n=0}^{N-t-1} w_n w_{n+t}, \quad t = 0, 1, \dots, N-1,$$

where δ_w is the sample variance of w_t . However, this conventional ACF is not robust to outliers and has $O(N^2)$ complexity. Instead, we propose to utilize the output of Huber-periodogram to obtain robust ACF with $O(N \log N)$ complexity. Specifically, since the time series is real-valued data, we can have the full-range periodogram

$$\bar{P}_k = \begin{cases} p_k^M & k = 0, 1, \dots, N-1 \\ \frac{(\sum_{k=0}^{N-1} x_{2k} - x_{2k+1})^2}{N'} & k = N \\ p_{N'-k}^M & k = N+1, \dots, N'-1 \end{cases}$$

Then, based on Wiener-Khinchin theorem [33], we obtain the robust ACF (denote as Huber-ACF) as

$$HuberACF(t) = \frac{p_t}{(N-t)p_0}, \quad t = 0, 1, \dots, N-1 \quad (19)$$

where p_t is the IDFT of \bar{P}_k defined as

$$p_t = \text{IDFT}\{\bar{P}_k\} = \frac{1}{\sqrt{N'}} \sum_{k=0}^{N'-1} \bar{P}_k e^{i2\pi kt/N'}. \quad (20)$$

Since we aim to detect single dominant periodicity in each level of wavelet coefficient, we summarize the peaks of the Huber-ACF through peak detection [23]. Then, we calculate the median distance of those peaks whose heights exceed the predefined threshold. Furthermore, based on the resolution of periodogram, i.e., the peak value of p_k^M at index k corresponds to period length in the range $[\frac{N}{k}, \frac{N}{k-1})$, the median distance of Huber-ACF peaks is the final period length only if it locates in the range of

$$R_k = \left[\frac{1}{2} \left(\frac{N}{k+1} + \frac{N}{k} \right) - 1, \dots, \frac{1}{2} \left(\frac{N}{k} + \frac{N}{k-1} \right) + 1 \right].$$

We denote the above described procedure as Huber-ACF-Med. By summarizing all the periods from the Huber-ACF-Med at different level of wavelet coefficients, we obtain the final periods of the original time series.

4 DEPLOYMENT AND APPLICATIONS

This algorithm is implemented and provided as a public online service at Alibaba Group. It has been applied widely in different business lines, including AIOps for Alicloud, business metrics monitoring, anomaly detection and forecasting, auto scaling of computing resources, and sales data mining for online retailing. The calling number of this service is over 0.3 million daily. Note that in practice the time series periodicity detection is not performed very frequently. Typically it is performed regularly in a relatively low frequency such as daily or weekly, or when a new task is launched.

Our periodicity detection algorithm plays an important role in Alibaba’s time series anomaly detection system. As different algorithms and strategies are customized for time series with and without periodicity, our periodicity is a core component to determine different pipelines and parameter settings. Another application is predictive auto scaling of computing resources across Alibaba Group. Predictive auto scaling monitors the usage of computing resources and automatically adjusts capacity to maintain steady, predictable performance at the lowest possible cost. It shines when the resource usage exhibits some patterns, particularly the periodic pattern. When the resource usage presents the periodic pattern, we can decompose the periodic components using our RobustSTL [31] algorithm, and reduce the resource when the periodic component is relatively small. Using our periodicity detection algorithm, our clients can easily identify these metrics on which auto scaling can be effectively applied.

5 EXPERIMENTS AND DISCUSSIONS

In this section, we study the proposed RobustPeriod algorithm empirically in comparison with other state-of-the-art periodicity detection algorithms on both synthetic and public real-world benchmark datasets. We also investigate how each component in RobustPeriod contributes to the final accurate detection.

5.1 Baseline Algorithms and Datasets

5.1.1 Existing Algorithms. We compare RobustPeriod with six algorithms, including three single-periodicity detection algorithm: 1) findFrequency [11]; 2) SAZED_{maj}; and 3) SAZED_{opt} [26], and three multi-periodicities detection algorithms: 4) Siegel [15, 24]; 5) AUTOPERIOD [18, 28]; and 6) Wavelet-Fisher [1]. As the trend component may bias the periodicity detection results significantly, we apply H-P filter to remove the trend component for all algorithms for a fair comparison in our experiments.

5.1.2 Synthetic Datasets. We generate synthetic time series of length 1000 with complex patterns, including 3 periodic components, multiple outliers, changing trend, and noises. Specifically, we first generate 3 sinusoidal waves with amplitude of 1 and period length of 20, 50, 100. Then we add a triangle signal with amplitude of 10 as trend. We add Gaussian noise and outliers in two scenarios: mild condition (noise variance $\sigma_n^2 = 0.1$, outlier ratio $\eta = 0.01$) and severe condition ($\sigma_n^2 = 2$ and $\eta = 0.2$). For single-period case, we only pick the periodic component with period 100. In all experiments, we randomly generate 1000 time series for evaluation. One synthetic data with mild condition is illustrated in Fig. 3.

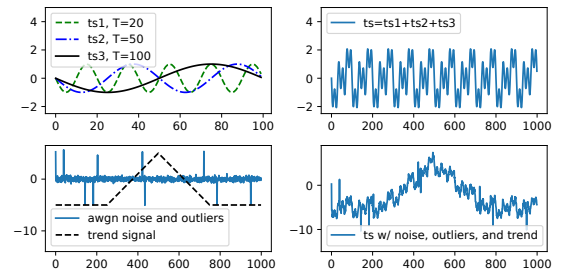


Figure 3: The generation of synthetic data with 3 periods.

5.1.3 Public Datasets. We use public single-period data from CRAN dataset [26], which contains 82 real-world univariate time series from a wide variety of domains, such as economic indicators, environmental measurements, etc. The length of these time series ranges from 16 to 3024, and their period length ranges from 2 to 52.

For public multiple-periods data, we select two Yahoo benchmark datasets, including the Yahoo-A3 and Yahoo-A4 [12]. These datasets contains 200 time series, and each time series contains 1680 points with three period lengths of 12, 24, and 168.

5.2 Comparisons with Existing Algorithms

5.2.1 Single-Periodicity Detection. We summarize the detection precision of single-periodicity detection algorithms on both synthetic and public CRAN datasets in Table 1, where $\pm 2\%$ indicates that detection is considered correct if the detected period length is within a 2% tolerance interval around the ground truth while $\pm 0\%$ indicates that we only consider exactly match. As the CRAN data contains both simple and complex periodic time series, the difference is not significant between different algorithms. For synthetic data, findFrequency cannot find the correct periodicity. The reason is that findFrequency fits an autoregression model for spectral density estimation when finding periodicity, while the added outliers make the autoregression model not accurate. In all cases, SAZED_{opt} outperforms SAZED_{maj} since the former uses its proposed optimal ensemble method while the later adopts a majority vote. Overall, RobustPeriod achieves the best performance.

5.2.2 Multi-Periodicity Detection. In multi-periodicity detection, we use F1 score to evaluate different algorithms as multiple periodicities are compared. The F1 scores of different algorithms on both synthetic and Yahoo datasets are summarized in Table 2. For synthetic data, Siegel algorithm has better performance than other existing algorithms, and also has relatively stable performance under $\pm 0\%$ and $\pm 2\%$ tolerance. While in Yahoo data, AUTOPERIOD has better performance than other existing algorithms. In both datasets, our RobustPeriod algorithm achieves the best performance.

In order to obtain more insights about the detection performance of difference algorithms, we plot the precision, recall, and F1 scores in Fig. 4. It can be observed that Siegel achieves the best recall but with relatively low precision. As Siegel is mainly based on the statistic test in the frequency domain, it seldom misses the true positive but often detects too many false positives. As Wavelet-Fisher decouples multi-periodicity signals by wavelet transform, it achieves relatively good performance. AUTOPERIOD achieves better performance as it utilizes both frequency and time domain information. Overall, our RobustPeriod algorithm has the best trade-off in performance, since it not only decouples the interference of multi-period but also utilizes both frequency and time domain information robustly.

5.3 Ablation Studies and Discussion

5.3.1 Ablation Studies. To further understand the contribution of each component in our RobustPeriod algorithm, we compare the performance of RobustPeriod with the following revisions: 1) **Huber-Fisher:** This algorithm replaces the vanilla periodogram in Fisher with Huber-periodogram; 2) **Huber-Siegel-ACF:** This algorithm also adopts Huber-periodogram when finding multiple period

Table 1: Precision comparisons of single-period detection algorithms on synthetic data and public CRAN data.

Algorithms	Synthetic Data				CRAN Data	
	$\sigma_n^2=0.1, \eta=0.01$		$\sigma_n^2=2, \eta=0.2$		$\pm 0\%$	$\pm 2\%$
	$\pm 0\%$	$\pm 2\%$	$\pm 0\%$	$\pm 2\%$		
findFrequency	0	0	0	0	0.44	0.44
SAZED _{maj}	0	0.32	0	0	0.49	0.49
SAZED _{opt}	0	0.96	0	0.54	0.55	0.56
RobustPeriod	0.83	1.0	0.44	0.98	0.56	0.57

Table 2: F1 score comparisons of multi-periodicity detection algorithms on synthetic and public Yahoo data.

Algorithms	Synthetic Data				Yahoo-A3		Yahoo-A4	
	$\sigma_n^2=0.1, \eta=0.01$		$\sigma_n^2=2, \eta=0.2$		$\pm 0\%$	$\pm 2\%$	$\pm 0\%$	$\pm 2\%$
	$\pm 0\%$	$\pm 2\%$	$\pm 0\%$	$\pm 2\%$				
Siegel	0.83	0.83	0.67	0.68	0.75	0.75	0.58	0.58
AUTOPERIOD	0.25	0.51	0.14	0.34	0.8	0.8	0.61	0.6
Wavelet-Fisher	0.5	0.75	0.48	0.72	0.5	0.76	0.49	0.73
RobustPeriod	0.84	0.96	0.72	0.93	0.82	0.85	0.82	0.89

Table 3: Ablation studies of the proposed RobustPeriod on synthetic data in severe condition ($\sigma_n^2=2, \eta=0.2$).

Algorithms	tolerance= $\pm 0\%$			tolerance= $\pm 2\%$		
	precision	recall	f1	precision	recall	f1
Huber-Fisher	0.91	0.3	0.46	0.89	0.3	0.45
Huber-Siegel-ACF	0.09	0.28	0.13	0.25	0.55	0.31
NR-RobustPeriod	0.71	0.6	0.64	0.96	0.79	0.85
RobustPeriod	0.76	0.7	0.72	0.98	0.91	0.93

candidates using Siegel’s test. Then, the candidates are validated by checking if they are located near the peaks of ACF as in AUTOPERIOD; 3) **NR-RobustPeriod:** This one is the non-robust version of RobustPeriod by using vanilla wavelet variance, periodogram, and ACF while sharing the same procedure as RobustPeriod.

Table 3 summarizes the detailed periodicity detection results (precision, recall, and F1 score) of the aforementioned revisions on the synthetic data under severe condition. It can be observed that all revisions have some performance degradation in comparison with RobustPeriod, and NR-RobustPeriod achieves the second best performance due to the same procedure as RobustPeriod.

We also compare these revisions with RobustPeriod on four representative real-world datasets as shown in Fig. 5. The first two datasets are from Alibaba¹ with single period. The last two datasets are from public tsdl library² with double periods. Table 4 summarizes the detection results of the aforementioned revisions. It can be observed that Huber-Fisher can only detect single dominant periodicity and cannot find the periodicity on Data-3 when the two periodic components have similar energy. In contrast, Huber-Siegel-ACF tends to generates too many false positives. NR-RobustPeriod could obtain the correct results in most cases, but fails on Data-1 where severe outliers exist. Overall, the proposed RobustPeriod achieve the best results.

5.3.2 Effectiveness of MODWT Decomposition. To further understand how RobustPeriod detects multiple periodicities, we plot the intermediate results in Fig. 6(a) for input time series in Fig. 3, where each row corresponds to a wavelet coefficient at a specific level,

¹These two datasets are trading volume and file exchange count from Alibaba Cloud, which are normalized for the purpose of anonymization.

²These two datasets are electricity usages from Time Series Data Library. v0.1.0. <https://pkg.yangzhuoranyang.com/tsdl/>

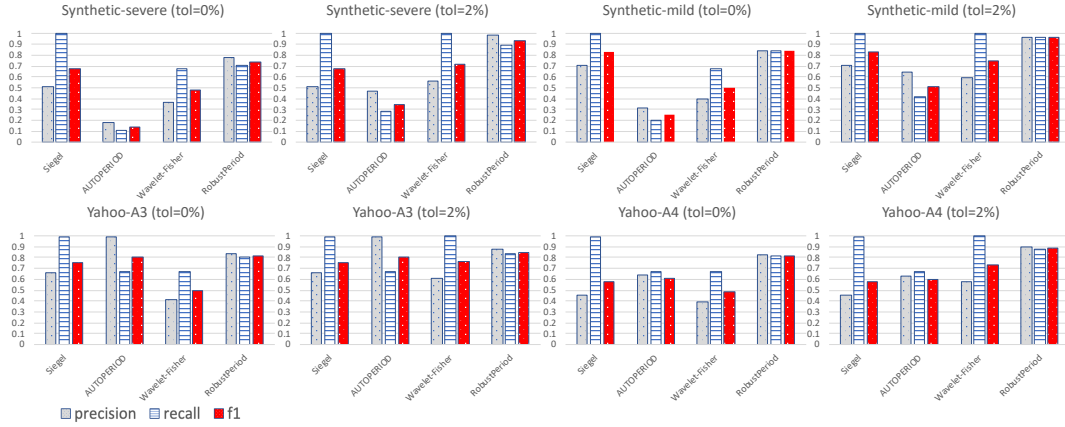


Figure 4: Detailed precision, recall, and F1 of multi-periodicity detection algorithms on synthetic data and public Yahoo data.

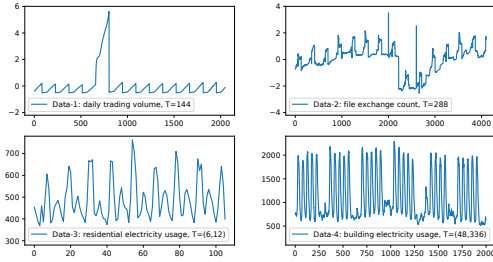


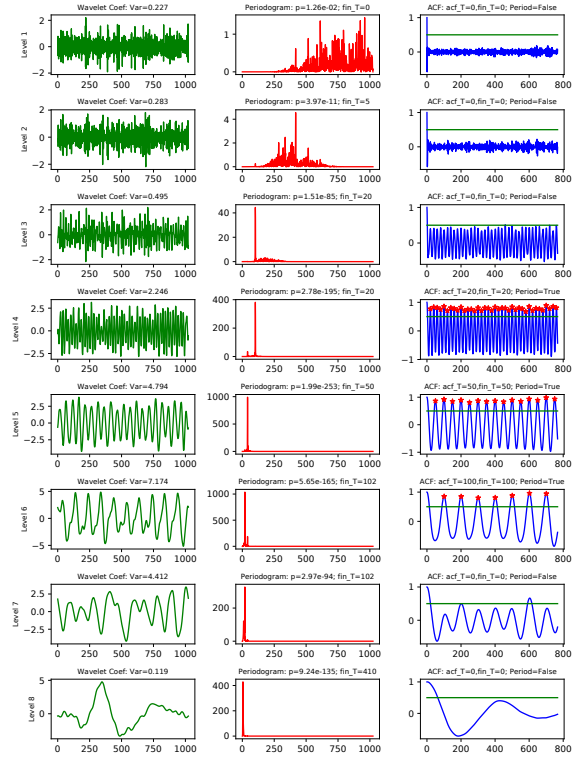
Figure 5: Real-world datasets: the first 2 datasets contain single period while the last 2 datasets have double periods.

Table 4: Comparisons of different periodicity detection algorithms on four real-world datasets.

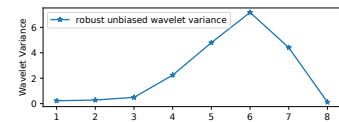
Algorithms	Data-1	Data-2	Data-3	Data-4
Huber-Fisher	146	293	NA	48
Huber-Siegel-ACF	(144,432,...)	(288,864,...)	(6,12)	(48,336,...)
NR-RobustPeriod	NA	286	(6,12)	(48,339)
RobustPeriod	144	288	(6,12)	(48,338)
Ground truth	144	288	(6,12)	(48,336)

and the first, second, and the last column are the wavelet coefficient, Huber-periodogram, and robust ACF, respectively. It can be observed that MODWT effectively decouples the interlaced periodicities. The Huber-periodogram and robust ACF effectively detect the periods of 20, 50, 100 at level 4, 5, 6, respectively. As a comparison, AUTOPERIOD cannot detect the period of 50 as the vanilla ACF does not have peak near 50 (the vanilla ACF drops near 50 due to the strong periodicities of 20 and 100). Fig. 6(b) plots the wavelets variances at different levels. It is clear that large wavelet variances correspond to strong periodic patterns at levels 4, 5, 6.

5.3.3 Effectiveness of Huber-Periodogram and Huber-ACF. To further understand how the single-periodicity detection works in RobustPeriod algorithm, we show an example in Fig. 7, where Fig. 7(a) shows the original single-period time series (length=102, period=24) before and after adding 2 outliers. Note that even without outliers, the two largest values in periodogram indicate the period can be 25.5 or 22.7 which is not correct due to the spectral leakage, while the location of ACF peaks (at 24, 48, and 72) can infer the right period length 24. The added 2 outliers severely affects periodogram



(a) Left to right: Wavelet coefficient, Huber-periodogram and ACF. The true period lengths 20, 50, 100 are correctly detected at level 4,5,6.



(b) Wavelet variance: the true periodic components located at levels 4,5,6 also have large wavelet variance.

Figure 6: Intermediate results of the RobustPeriod.

and ACF as shown in Fig. 7(b), which brings difficulties to detect the correct periodicity. The use of LAD-periodogram [13] can somehow obtain better periodogram but the corresponding ACF is still

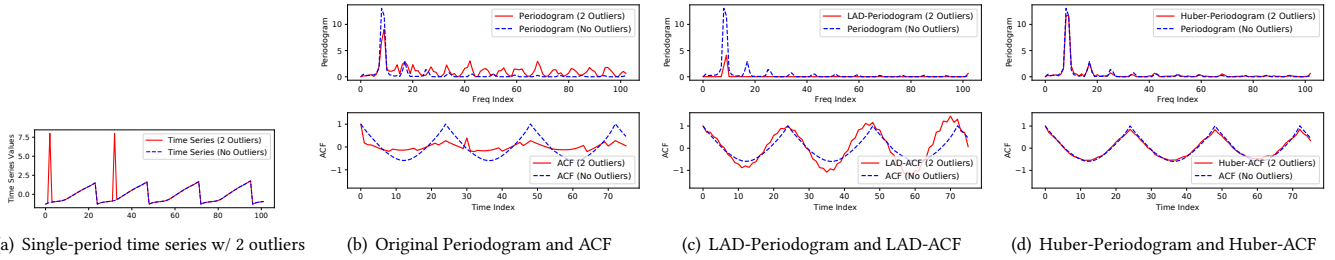


Figure 7: Comparisons of different Periodogram and ACF schemes for single-period detection.

affected as shown in Fig. 7(c). In contrast, our proposed Huber-periodogram and Huber-ACF can obtain the same peak locations as the original periodogram and ACF without outliers as shown in Fig. 7(d), which leads to the correct periodicity detection.

6 CONCLUSION

In this paper we propose a new periodicity detection method Robust-Period by mining periodicities from joint time-frequency domain. It utilizes MODWT to isolate the interlaced multiple periodicities successfully. To identify the potential periodic pattern at different levels, we apply the robust wavelet variance to select the most promising ones. Furthermore, we propose Huber-periodogram and the corresponding ACF to detect periodicity accurately and robustly. The theoretical properties of Fisher’s test on Huber-periodogram are proved. In the future, we plan to apply it in more time series related tasks inside and outside Alibaba.

REFERENCES

- [1] Abdullah Almasri. 2011. A New Approach for Testing Periodicity. *Communications in Statistics - Theory and Methods* 40, 7 (2011), 1196–1217.
- [2] Miguel A Arcones. 2001. Asymptotic distribution of regression M-estimators. *Journal of statistical planning and inference* 97, 2 (2001), 235–261.
- [3] George EP Box, Gwilym M Jenkins, Gregory C Reinsel, and Greta M Ljung. 2015. *Time series analysis: forecasting and control*. New York.
- [4] Stephen Boyd, Neal Parikh, Eric Chu, Borja Peleato, Jonathan Eckstein, et al. 2011. Distributed optimization and statistical learning via the alternating direction method of multipliers. *Foundations and Trends in Machine learning* 3, 1 (2011).
- [5] I Daubechies. 1992. *Ten Lectures on Wavelets*. Society for Industrial and Applied Mathematics.
- [6] Mohamed G Elfeky, Walid G Aref, and Ahmed K Elmagarmid. 2005. WARP: time warping for periodicity detection. In *Fifth IEEE International Conference on Data Mining (ICDM’05)*. IEEE, 1–8.
- [7] Ronald Aylmer Fisher. 1929. Tests of significance in harmonic analysis. *Proceedings of the Royal Society of London. Series A, Containing Papers of a Mathematical and Physical Character* 125, 796 (1929), 54–59.
- [8] Matthew J Graham, Andrew J Drake, S G Djorgovski, Ashish A Mahabal, et al. 2013. A comparison of period finding algorithms. *Monthly Notices of the Royal Astronomical Society* 434, 4 (aug 2013), 3423–3444.
- [9] Robert J Hodrick and Edward C Prescott. 1997. Postwar US business cycles: an empirical investigation. *Journal of Money, Credit, and Banking* (1997), 1–16.
- [10] Peter J. Huber and Elvezio M. Ronchetti. 2009. *Robust Statistics* (2nd ed.). John Wiley & Sons, New Jersey.
- [11] Rob J Hyndman, George Athanasopoulos, Christoph Bergmeir, Gabriel Caceres, Leanne Chhay, Mitchell O’Hara-Wild, Fotios Petropoulos, and Slava Razbash. 2019. Package ‘Aforecast’. (2019).
- [12] Nikolay Laptev, Saeed Amizadeh, and Ian Flint. 2015. Generic and Scalable Framework for Automated Time-series Anomaly Detection. In *Proceedings of the 21th ACM SIGKDD International Conference on Knowledge Discovery and Data Mining (KDD ’15)*. ACM, 1939–1947.
- [13] Ta-Hsin Li. 2008. Laplace Periodogram for Time Series Analysis. *J. Amer. Statist. Assoc.* 103, 482 (jun 2008), 757–768.
- [14] Ta-Hsin Li. 2010. A nonlinear method for robust spectral analysis. *IEEE Transactions on Signal Processing* 58, 5 (2010), 2466–2474.
- [15] Ta-Hsin Li. 2016. *Time series with mixed spectra* (1st ed.). Chapman and Hall/CRC, Boca Raton, FL.
- [16] Zhenhui Li, Jingjing Wang, and Jiawei Han. 2012. Mining event periodicity from incomplete observations. In *Proceedings of the 18th ACM SIGKDD international conference on Knowledge discovery and data mining*. ACM, 444–452.
- [17] C L Mallows. 1967. Linear Processes Are Nearly Gaussian. *Journal of Applied Probability* 4, 2 (1967), 313–329.
- [18] Theophano Mitsa. 2010. *Temporal Data Mining* (1st ed.). Chapman and Hall/CRC, Boca Raton, FL.
- [19] Srinivasan Parthasarathy, Sameep Mehta, and Soundararajan Srinivasan. 2006. Robust periodicity detection algorithms. In *Proceedings of the 15th ACM international conference on Information and knowledge management*. ACM, 874–875.
- [20] Donald B Percival and Andrew T Walden. 2000. *Wavelet methods for time series analysis*. Vol. 4. Cambridge university press, New York.
- [21] Faraz Rasheed and Reda Alhajj. 2013. A framework for periodic outlier pattern detection in time-series sequences. *IEEE Transactions on Cybernetics* 44, 5 (2013), 569–582.
- [22] Galen Reeves, Jie Liu, Suman Nath, and Feng Zhao. 2009. Managing Massive Time Series Streams with Multi-Scale Compressed Trickle. *Proc. VLDB Endow.* 2, 1 (Aug. 2009), 97–108.
- [23] Felix Scholkemann, Jens Boss, and Martin Wolf. 2012. An Efficient Algorithm for Automatic Peak Detection in Noisy Periodic and Quasi-Periodic Signals. *Algorithms* 5, 4 (2012), 588–603.
- [24] Andrew F Siegel. 1980. Testing for Periodicity in a Time Series. *J. Amer. Statist. Assoc.* 75, 370 (jun 1980), 345–348.
- [25] Marina Theodosiou. 2011. Forecasting monthly and quarterly time series using STL decomposition. *International Journal of Forecasting* 27, 4 (2011), 1178–1195.
- [26] Maximilian Toller, Tiago Santos, and Roman Kern. 2019. SAZED: parameter-free domain-agnostic season length estimation in time series data. *Data Mining and Knowledge Discovery* (2019).
- [27] Michail Vlachos, Christopher Meek, Zografoula Vagena, and Dimitrios Gunopulos. 2004. Identifying similarities, periodicities and bursts for online search queries. In *Proceedings of the 2004 ACM SIGMOD international conference on Management of data*. ACM, 131–142.
- [28] Michail Vlachos, Philip Yu, and Vittorio Castelli. 2005. On periodicity detection and structural periodic similarity. In *Proceedings of the 2005 SIAM International Conference on Data Mining*. SIAM, 449–460.
- [29] DeLiang Wang and Guy J. Brown. 2006. *Computational Auditory Scene Analysis: Principles, Algorithms, and Applications*. Wiley-IEEE Press.
- [30] Wang, J., Chen, T., and Huang, B. 2006. Cyclo-period estimation for discrete-time cyclo-stationary signals. *IEEE Transactions on Signal Processing* 54, 1 (Jan 2006), 83–94.
- [31] Qingsong Wen, Jingkun Gao, Xiaomin Song, Liang Sun, Huan Xu, and Shenghuo Zhu. 2019. RobustSTL: A Robust Seasonal-Trend Decomposition Algorithm for Long Time Series. In *AAAI*. 1501–1509.
- [32] Sofia Wichert, Konstantinos Fokianos, and Korbinian Strimmer. 2004. Identifying periodically expressed transcripts in microarray time series data. *Bioinformatics* 20, 1 (2004), 5–20.
- [33] Norbert Wiener. 1930. Generalized harmonic analysis. *Acta Math.* 55 (1930), 117–258.
- [34] Rand R Wilcox. 2017. *Introduction to Robust Estimation and Hypothesis Testing* (4th ed.). Academic press, New York.
- [35] Quan Yuan, Jingbo Shang, Xin Cao, Chao Zhang, Xinhe Geng, and Jiawei Han. 2017. Detecting Multiple Periods and Periodic Patterns in Event Time Sequences. In *Proceedings of the 2017 ACM on Conference on Information and Knowledge Management*. ACM, 617–626.
- [36] Li Zhu, Yanxin Wang, and Qibin Fan. 2014. MODWT-ARMA model for time series prediction. *Applied Mathematical Modelling* 38, 5 (2014), 1859–1865.